University of Glasgow | Experimental Particle Physics

GLAS-PPE/2008-26
31th August 2008

Department of Physics and Astronomy
Experimental Particle Physics Group
Kelvin Building, University of Glasgow,
Glasgow, G12 8QQ, Scotland
Telephone: +44 (0)141 330 2000 Fax: +44 (0)141 330 5881

Synchrotron tests of a 3D Medipix2 X-ray detector

D. Pennicard[1], J. Marchal[2], C. Fleta[1], G. Pellegrini[3], M. Lozano[3],
C. Parkes[1], N. Tartoni[2], D. Barnett[2], I. Dolbnya[2],
K. Sawhney[2], R. Bates[1], V. O'Shea[1], V. Wright[4]

[1] University of Glasgow, Department of Physics and Astronomy, Glasgow, UK, G12 8QQ
[2] Diamond Light Source Ltd, Harwell Science and Innovation Campus, Oxfordshire, UK, OX11 0DE
[3] Instituto de Microelectronica de Barcelona, IMB-CNM-CSIC, 08193 Bellaterra, Barcelona, Spain
[4] Science and Technology Facilities Council, Polaris House, North Star Ave., Swindon, UK

Abstract

Three-dimensional (3D) photodiode detectors offer advantages over standard planar photodiodes in a range of applications, including X-ray detection for synchrotrons and medical imaging. The principal advantage of these sensors for X-ray imaging is their low charge sharing between adjacent pixels, which improves spatial and spectral resolution.

A 'double-sided' 3D detector has been bonded to a Medipix2 single-photon-counting readout chip, and tested in a monochromatic X-ray beam at the Diamond synchrotron. Tests of the 3D detector's response spectrum and its Line Spread Function have shown that it has substantially lower charge sharing than a standard planar Medipix2 sensor. Additionally, the 3D detector was used to image diffraction rings produced by a powdered silicon sample, demonstrating the detector's use in a standard synchrotron experiment.

Submitted to Journal of Synchrotron Radiation

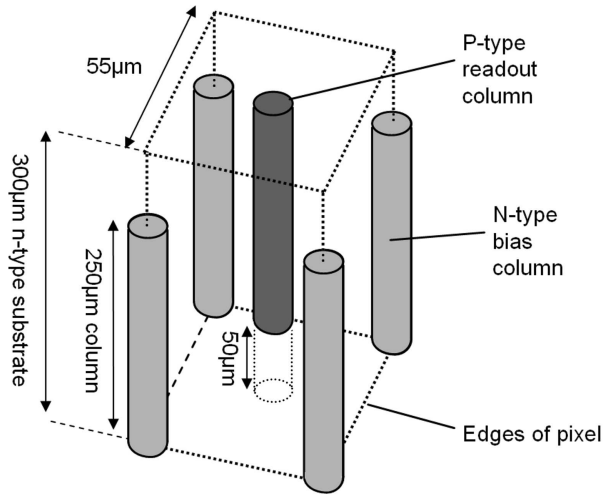

Figure 1: The basic structure of one pixel of a double-sided 3D detector. Dimensions match the device tested in this paper.

1 Introduction

The high-intensity X-ray beams produced by new synchrotrons such as Diamond Light Source can be used to improve the speed and quality of X-ray diffraction experiments. However, in order to fully exploit these new light sources, high-performance X-ray detectors are also needed [1]. New X-ray detectors can also be applied to other important applications, such as medical imaging.

In many of these applications, high-resolution X-ray images are required. However, X-ray detectors with small pixel sizes suffer from charge-sharing effects, which tend to blur the image and reduce spectral resolution [2]. 3D detectors, proposed by S. Parker et al. [3], can potentially improve X-ray imaging by reducing these effects.

1.1 3D detectors

A 3D detector is a specialised variety of silicon photodiode detector. A regular photodiode has a planar structure, with p- and n-type electrodes on the front and back surfaces of a silicon substrate. In a 3D detector, these electrodes are replaced by columns of p- and n-type material, passing through the thickness of the substrate. In a "double-sided" 3D detector [4], the columns of one doping type are etched from the front surface, and individually connected to readout electronics, and the other columns are etched from the back surface, and used to bias the detector. A simple diagram of one pixel in a double-sided 3D detector, with dimensions matching the device tested here, is shown in Fig. 1. The columns are fabricated by etching holes in the wafer, then doping inside the holes. Frequently, the holes are completely or partially filled with polysilicon [5].

The electrode spacing in a planar photodiode is determined by the substrate thickness - typically, at least a few hundred microns. By using the 3D structure, it becomes possible to combine a reasonably thick substrate with an extremely small electrode spacing - as little as a few tens of microns. This dramatically reduces the depletion voltage and the collection time of the detector, making these detectors useful for future high-energy physics applications [6]. For X-ray imaging, the most important advantage of the 3D structure is reduced charge sharing, as demonstrated by simulation studies [7]. Firstly, the fast charge collection in a 3D detector means that there is less time for the cloud of charge carriers to spread by diffusion. Secondly, the electric field pattern in the device causes the carriers to drift horizontally towards the readout columns, away from the pixel boundaries.

An additional benefit of 3D detectors is that the fabrication tools used to produce the columns can also be used to add an "active edge" electrode to the sensor, reducing the dead area at the edge to as little as 5μm [8]. In contrast, standard photodiodes with saw-cut edges have a dead area of at least 100μm. So, active edges make it possible to tile the sensors over a large area, with minimal dead space between them. Note that the first fabrication run of Medipix2 3D detectors tested here did not include active edges.

1.2 Medipix2 single-photon-counting readout chip

A photodiode detector has a separate readout channel for each pixel. To read out the detector, it is bump-bonded to a chip that amplifies the signal from each channel, then applies more sophisticated processing. The Medipix2 readout chip [9] used here is specifically designed for X-ray detection, in applications such as medical imaging. It has a 256 by 256 array of square, 55μm pixels, covering a total area of 14mm by 14mm.

Whenever a hit occurs on a Medipix pixel, the signal is compared to high and low signal thresholds set by the user. If the signal falls between the two thresholds, a counter within the pixel is incremented. This allows the chip to count the individual X-ray photons hitting each pixel during an exposure. As a result, the detector has a high count rate and a large, linear dynamic range, and it is also largely unaffected by electronic noise. These advantages are useful for synchrotron diffraction experiments, because the brightest diffraction spots in an image may have extremely high count rates but the rate in the weakest spots may be orders of magnitude lower.

In a single-photon-counting detector, charge-sharing can reduce the image quality in various ways. Firstly, depending on the threshold setting, charge-shared events can either be missed (reducing the signal) or produce hits in more than one pixel (blurring the image). If the incident beam contains a wide spectrum, both these effects may occur. Additionally, charge-sharing reduces the detector's ability to distinguish between photons of different energy - for example, to reject Compton scattering or fluorescence from a sample [2].

2 Detectors, apparatus and preliminary tests

2.1 Detectors

The 3D detector tested here is a double-sided 3D detector, fabricated by IMB-CNM as described in [4]—see Fig. 1. The detector has a 300μm-thick n-type substrate. The columns fabricated in the substrate are 250μm long (i.e. they do not pass through the full substrate thickness) and are 10μm in diameter. Boron-doped p-type columns extend from the front surface into the bulk silicon, and have individual bump-bond pads. The phosphorus-doped n-type columns extending from the back surface are connected together by layers of polysilicon and metal, and are used for biasing. The pitch between adjacent columns of the same type is 55μm, to match the pixel size of Medipix2. After fabrication, the sensor was bump-bonded to a Medipix2 chip by VTT, and mounted on a chipboard. VTT have previous experience of producing simpler "semi-3D" sensors and bonding them to Medipix2 [10].

For comparison, a standard 300μm-thick p-on-n planar detector was also tested.

2.2 Data acquisition

The Medipix2 chipboards were read out using Medipix2 USB interfaces, produced by IEAP, Czech Technical University, Prague [11]. This interface powers the chipboard and reads out the detector using a USB connection. It also has a built-in high voltage source for biasing the detector. During the beam test, the detectors inside the beam area were connected to a PC outside via a USB extender.

2.3 Beamline and test setup

The X-ray tests were done at beamline B16 at the Diamond Light Source, which is designed to test new detectors, experimental techniques and optics. The beamline can provide white or monochromatic beam; during the tests, only the monochromatic beam was used, in the range 12-20keV. More information on the beamline is available from [12].

The Medipix2 detectors were each mounted in an aluminium test box with a 50μm-thick aluminized Mylar window in front of the detector active area. During the tests, they were mounted on a remotely-controlled XY stage, allowing them to be moved in and out of the beam without having to re-open the beam area.

2.4 Preparation for tests

During all the tests, the 3D detector was biased to 21.5V and the planar detector was biased to 100V, ensuring that both were fully depleted.

Before testing the detectors, it was necessary to perform threshold equalisation. Medipix2 uses a global low threshold (THL) to determine whether or not a hit is registered. Each individual pixel has three THL adjust bits which are used to improve the uniformity of the threshold across the detector [9]. Because the Medipix2 chip is bipolar, the noise level lies in the middle of the chip's dynamic range, and so the thresholds could be equalised using the centroid of the noise on each channel. This process also produced a histogram of the centroid

position for each pixel after equalisation; the peak of this histogram gave the THL value corresponding to zero signal. Although the chip also has a high threshold, only the low threshold was used.

Since the beam profile was non-uniform, motorised tungsten slits were used to give a square beam spot, slightly smaller than the area of the detector. This ensured that we consistently imaged the same area of the beam when switching between the two detectors.

2.5 Electronic noise, pixel masking, and radiation damage

Since it counts individual photons, rather than integrating the signal detected over the acquisition time, the Medipix2 chip is not affected by electronic noise in a conventional way. However, if the noise fluctuations are large enough, a pixel can register false hits. This will of course depend on the threshold setting.

As a test of detector noise, the low threshold was scanned through a range of values without any beam present, with 0.1s acquisitions at each setting. At each setting, the 3D detector tended to show more noisy pixels than the planar detector. As a representative example, the threshold was set to 6keV, i.e. half the energy of the lowest-energy beam used in the tests. (Section 3 describes how the energy calibrations were found.) The 3D detector had 4 pixels with extremely high noise counts of over 10,000, and 66 moderately noisy pixels with over 100 counts. In contrast, the planar detector had only 1 pixel with more than 100 counts. The increased noise on the 3D detector may be related to its relatively high capacitance per pixel [13]. However, the noise can also depend on the individual Medipix2 readout chip. During the data analysis, noisy pixels were appropriately masked.

After making the spectra measurements, but before the Line Spread Function and diffraction experiments, both Medipix2 readout chips showed signs of radiation damage. Firstly, the number of noisy pixels had increased, and secondly, when the threshold equalisations were repeated, the THL adjust values had changed for some of the pixels. The pixels which hadn't been exposed to the beam were unaffected. This damage will be due to the production of fixed charges in the gate oxides on the readout chip, which alters the behaviour of some of the transistors. The damage was unexpectedly high, and may have been caused by accidentally exposing the detectors to the direct X-ray beam when changing attenuators.

3 Beam spectra measurements with Medipix2

After setting the X-ray beam to 15keV, the response spectrum of each detector was tested. This was done by taking images at a series of consecutive low threshold (THL) values ranging from above the beam energy down to the noise level. An acquisition time of 0.5s was used at each step - this was chosen to ensure a high count in each pixel, without reaching the Medipix2 chip's maximum count. As mentioned previously, the 3D and planar detectors were biased to 21.5V and 100V.

Then, the total number of counts was calculated for each image (excluding noisy pixels), producing an integral spectrum of counts vs threshold setting. This was then differentiated to find the differential spectrum measured by each detector. This spectral measurement was repeated a total of 10 times, and the mean spectrum found. The standard error on each point in the spectrum was also calculated.

At this point, the spectrum simply gave the signal at each THL setting. In order to calibrate the detector, the tests were repeated at 12keV and 20keV. The peak in each spectrum was found by using a Gaussian fit. Having obtained the THL values corresponding to these energies, and also the "zero signal" THL value from the threshold equalisation, a linear least-squares fit was made to these points to find the calibration for each detector. This was then applied to the spectra. The change in energy corresponding to a step in THL was very similar on the two detectors, but the "zero signal" THL levels were different. This effect has been seen previously on other Medipix2 sensors—for example, in [10].

Figure 2 shows the spectrum obtained from the 3D detector with the 15keV beam, including the Gaussian peak fit and the standard error on each data point. In addition to the peak, lower energy "hits" can be seen, due to some X-rays being charge-shared between pixels. Before fitting the Gaussian to the peak, the steepest point on the low-energy edge was found, and the fit was only applied to the data at higher energies. This prevented the charge-shared signal from affecting the fit.

Figure 3 shows the results from the 3D and planar detectors superimposed, with a Gaussian fit to each peak. It can clearly be seen that the planar detector has a smaller peak and a greater charge shared signal, giving a poorer spectrum as a result.

The onset of false counts due to noise occurs sooner on the 3D detector than on the planar. However, in all of these tests the 3D and planar detectors give very similar peak widths. Since the beam is very monochromatic, the peak width reflects aspects of detector response such as electronic noise and threshold dispersion. So, the earlier onset of noise on the 3D detector might only be due to poor noise performance in a small fraction of the pixels.

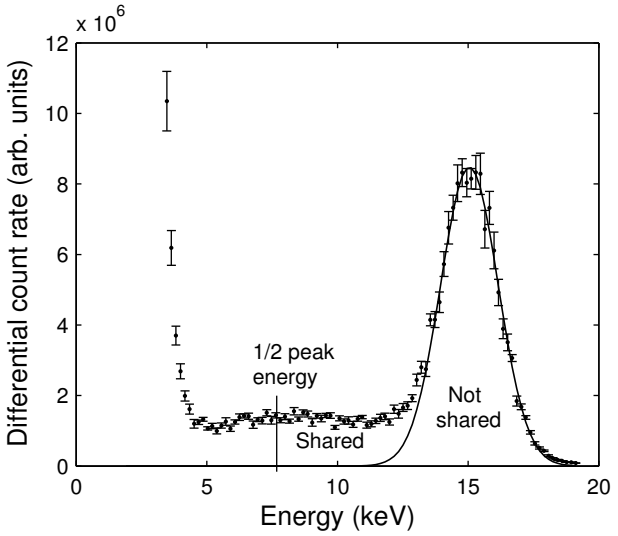

Figure 2: Spectrum from the 15keV beam measured by the 3D detector.

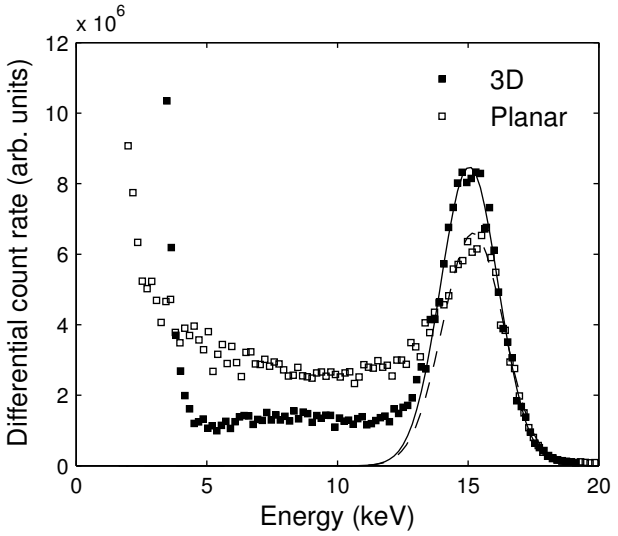

Figure 3: Comparison of 15keV beam spectra measured by 300μm 3D and planar detectors, showing greater charge sharing on the planar sensor.

Table 1: Results from spectra measurements on planar and 3D detectors.

Energy (keV)	3D - % charge shared	Planar - % charge shared	(Counts 3D) / (Counts planar) at $E_{beam}/2$
12	26.1	37.1	0.856
15	24.0	45.0	0.892
20	20.1	36.3	0.827
Mean	23.4	39.5	0.858

To determine the total number of photons detected by each sensor, the count rate was found with the low threshold set to half the beam energy. This value will include as many of the charge-shared hits as possible, without any hits being counted twice in adjacent pixels. Only the small number of hits shared equally between 3 or 4 pixels will be missed. By integrating the total number of hits in the Gaussian fitted to the peak, the number of non-charge-shared hits was also found. So, the proportion of charge-shared hits on the detector could be found for each data set. Fig. 2 illustrates this.

For each beam energy, Table 1 shows the proportion of charge-shared events on each detector, and the relative number of hits seen on the two detectors at half the peak energy. To make the latter comparison, the total counts were adjusted to take into account small changes in the beam intensity as the electron current in the synchrotron decayed. The mean results for the three tests are also shown. The 3D detector has a substantially lower proportion of charge-shared hits; 23.4%, compared to 39.5% for the planar sensor. The results show no clear pattern with energy. There is greater variation in the results from the planar sensor, probably because the larger number of charge-shared events makes it harder to get an accurate Gaussian fit to the peak.

Additionally, when the threshold is set to half the peak energy, the count rate on the 3D detector is only 86% compared to the planar detector. This suggests that the 3D detector has a smaller sensitive volume. This may at least partly be due to loss of signal from hits occurring in the electrode columns, which occupy about 5% of the device volume, or 10%, if we include the heavily-doped region around the columns. Variations in substrate thickness could also affect the results. The nominal substrate thickness is $300\pm15\mu$m, which would correspond to a variation of $\pm5\%$ in the active volume of each detector.

4 Measuring Line Spread Function using an edge

Next, the Line Spread Function (LSF) was measured for the two detectors, using a 12keV beam. The LSF is the response of the detector to an input signal consisting of an extremely narrow line. It is equivalent to the response of a single pixel when a narrow line is scanned across it. The LSF was found by measuring the Edge Spread Function (ESF)—the response to a sharp edge—then differentiating it, using a similar method to [14].

Firstly, a thin lead edge on a glass slide was placed over each detector, at a shallow angle to the horizontal (about 2 degrees). Across any individual pixel, the edge is virtually horizontal, but the tilt is large enough to ensure that the distance from the edge to the centre of each pixel varies across the detector. This makes it possible to obtain the "oversampled" ESF and LSF with a step size much smaller than the pixel spacing itself.

Ideally, this experiment should be carried out using a perfectly uniform X-ray source. To compensate for the non-uniformity of the X-ray beam used here, images were taken both with the glass slide mounted on the detector and with it removed. During analysis, the count rate seen in each pixel in the edge image was divided by the count rate without the edge in place. As well as helping to compensate for the beam's non-uniformity, this will also compensate for variations in the response of individual pixels (flat-field correction). These images were taken for both the 3D and planar detectors at a range of different threshold settings. Each measurement consisted of 100 images taken with a 2.5s acquisition time, which were then averaged.

Firstly, the position of the edge in the image was found. This was done by looking at each column of pixels in the image and finding the Y-position where the count rate was halfway between the maximum and minimum signal level, using interpolation to get sub-pixel precision. Then, a linear fit was made to the resulting data points.

Next, the perpendicular distance from the line to the centre of each pixel was calculated. From this, a scatter plot of the count rate against the distance from the edge was constructed—an example from the 3D detector is shown in Fig. 4. Pixels at the same distance from the line can have different values, due to any variations in pixel response or beam intensity still present applying the correction. So, to obtain the Edge Spread Function from this data, smoothing was applied using a locally weighted linear regression (LOESS) fit. For each point in the original data, this applies a linear fit to the surrounding data points, with the weighting of each point falling rapidly with distance. The smoothing also assigns zero weight to points more than 6 standard deviations from the line, to reject outliers. As can be seen in Fig. 4, this gives a smoothly varying ESF.

The ESF was interpolated, to give equally-spaced data points, then differentiated, to obtain the Line Spread Function. Once again, some smoothing had to be applied, because the differentiation enhanced small variations in the ESF data. An example of the LSF before and after smoothing is shown in Fig. 5. This shows the response of a pixel, with steep rising and falling edges and a plateau in the centre. Note that both the plateau and the region to the right show some undulation. This is most likely due to variations in the beam profile which could not be fully corrected. Unfortunately, this prevents us from seeing if there is any fine structure in the "plateau" region due to the readout column. However, the rising and falling edges of the LSF are a good source of information.

The LSF was found for the two detectors at a range of threshold settings. Each data set gave a LSF with

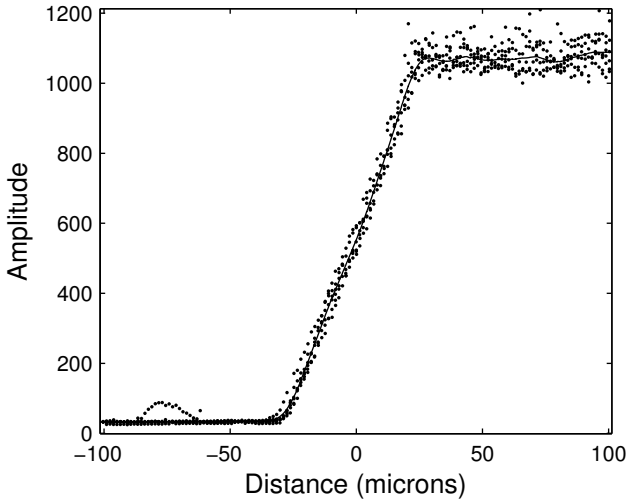

Figure 4: Edge Spread Function measured by the 3D detector at threshold setting THL385 (6.7keV), showing individual pixel values and the smoothed fit.

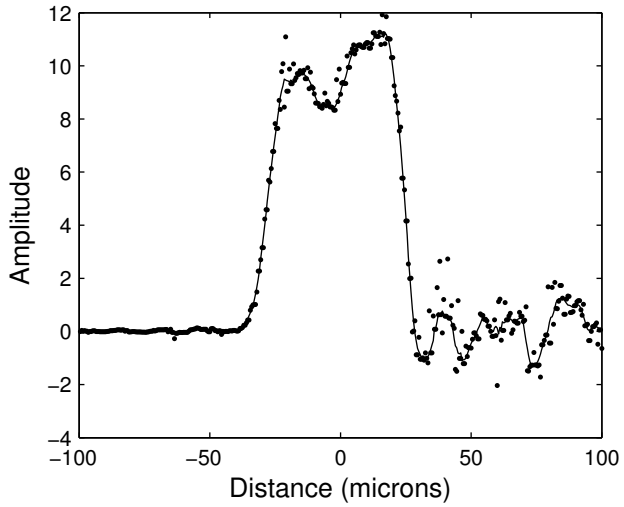

Figure 5: Line Spread Function measured by the 3D detector at threshold setting THL385 (6.7keV), before and after smoothing.

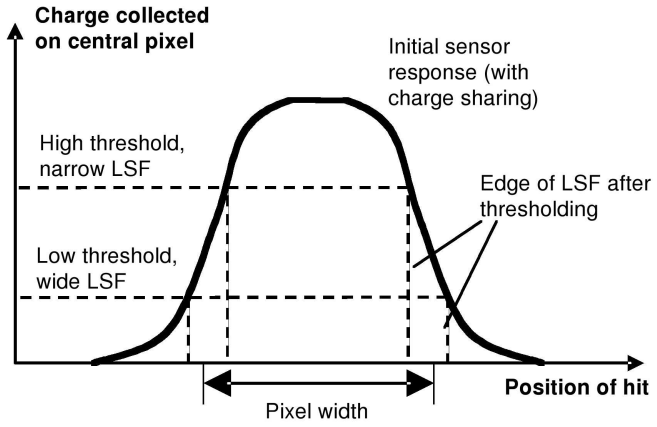

Figure 6: Diagram showing how charge sharing and varying thresholds affect the LSF from a single-photon-counting chip.

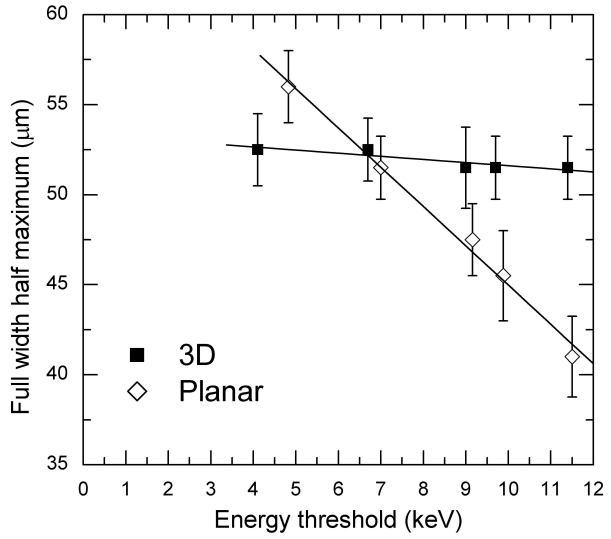

Figure 7: Variation in the full width half maxima of LSFs measured at different threshold settings using a 12keV beam, for both 3D and planar detectors. The planar detector has greater variation, indicating higher charge sharing.

steep rising and falling edges, and a plateau, but the width of the LSF showed some variation with the threshold setting. Consider the response of the detector system to monochromatic X-rays. The signal amplitude produced by a pixel of a photodiode detector will vary smoothly with the X-ray hit position as shown in Fig. 6. The steepness of the rising and falling edges will depend on the amount of charge sharing. When the signal is passed to the Medipix2 chip, it will either register a hit or not, depending on the signal amplitude and the threshold setting. So, the LSF obtained from the Medipix2 with a monochromatic beam will tend to have sharp edges, regardless of charge sharing. However, the width of the LSF will vary with the threshold setting, and this variation will be greater if there is high charge sharing.

So, for each data set, the full-width-half-maximum (FWHM) of the LSF was found. As an estimate of the error in this measurement, the widths of the LSF at 40% and 60% of the plateau level were also calculated. The resulting full width half maxima, with these errors, are plotted against the threshold setting in Fig. 7.

The FWHM of the 3D detector shows very little variation with the threshold setting - in the range of thresholds tested here, it only varies by 1.5um, with a value of 52.5μm when the threshold is set to half the 12keV beam energy. In contrast, the planar detector's response varies by 15μm across the threshold range, with 53.5μm width at half the beam energy. So, this shows that the 3D detector has much lower charge sharing at the edges of the pixel. On both detectors, the width at half the beam energy is a little narrower than the 55μm pixel size, which is reasonable; since we have 2D pixels, with increased charge sharing at the corners, this causes the 1-dimensional LSF profile to become a little narrower.

5 Silicon powder diffraction experiment

After making these direct measurements of the two detectors' performance, the detectors were then used in an experiment to measure powder diffraction patterns. A capillary tube containing a reference sample of powdered silicon (SRM 640c) was placed in a focused 15keV beam, producing a series of diffraction rings. The sample was 24cm from the detector stage. Since the diffraction rings covered a large angular range, and each Medipix2 image covered only 14mm by 14mm, a series of images were taken with the detectors while moving the stage in 10mm increments along the X-direction. If a ring was seen on a detector, 10 images were taken (each with a 10s shutter time) and averaged; if not, only one image was taken. During these measurements, the detection threshold on each detector was set to 7.5keV, half the beam energy.

An example image, showing the innermost diffraction ring as seen by the 3D detector, is shown in Fig. 8. Noisy pixels, identified by taking images without the beam present (see section 2.5), were replaced by the median count rate from the neighbouring pixels. The detector is only large enough to image a segment of the ring, but the curvature is still visible. Also, it can clearly be seen that the ring is composed of a series of diffraction spots, produced by individual crystals in the powdered silicon sample. To get the response of the detector across the full angular range, the images were cropped and stitched together appropriately. The result

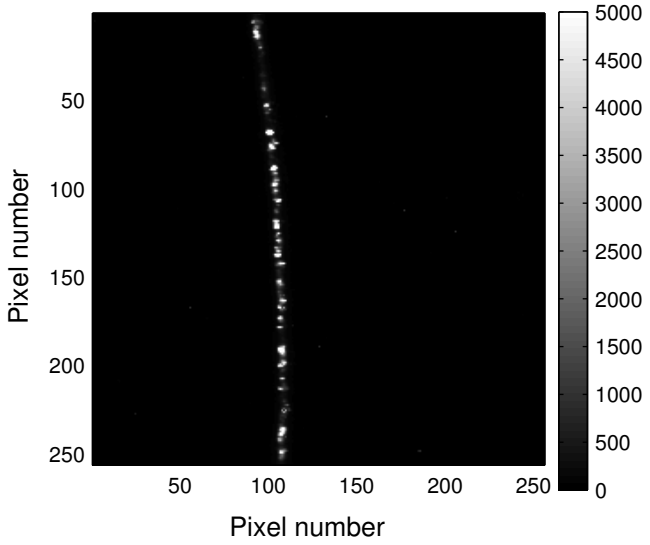

Figure 8: Image of a diffraction ring from a powdered silicon sample, taken with the 3D detector. The greyscale shows the counts per pixel.

for the 3D detector is shown in Fig. 9, with the left-hand side of the image having the smallest angle relative to the incoming beam. Seven diffraction rings can be seen, along with a background which decreases as the diffraction angle increases.

Next, a projection was made of the mean number of counts per pixel versus the distance from the centre of the diffraction pattern. This was found by making a circular fit to the innermost diffraction ring, calculating the distance of each pixel from the centre of this ring, and binning the results in steps of half a pixel width. This "distance" variable was then used to find the corresponding angle of the diffracted beam, relative to the incoming beam (i.e. 2θ).

The diffraction results for the 3D detector are shown in Fig. 10. The angles of the seven diffraction rings seen here are a good match to the expected Bragg reflections produced by the silicon crystal planes (1 1 1) to (3 3 3). These were calculated using NIST data [15].

Fig. 11 shows the first peak in the projection, expressed in terms of the distance measured on the detector rather than the angle. The full-width half maximum of this peak is 3.5 pixels. Given the relatively large width of the peaks, when the experiment was repeated using the planar sensor there was no visible difference between the peak shapes seen on the two sensors.

6 Conclusions

The first Medipix2 3D sensor has been successfully fabricated, tested, and used in a standard X-ray diffraction experiment. Measurements of the 3D detector's spectral response show significantly less charge sharing than an equivalent planar detector—23.4%, compared to 39.5%. Likewise, measurements of the width of the Line Spread Function using a monochromatic beam show little variation with threshold setting. This is also evidence of low charge sharing at the pixel edges. Currently, more Medipix2 3D detectors are being produced, in order to optimise the fabrication process and provide more sensors for use in larger detector systems.

Acknowledgements

This work has been supported by the Spanish Ministry of Education and Science through the GICSERV program "Access to ICTS integrated nano- and microelectronics cleanroom". This work was carried out in the context of the RD50 collaboration. Thanks also to Hiten Patel at Diamond Light Source for help during initial tests of these sensors.

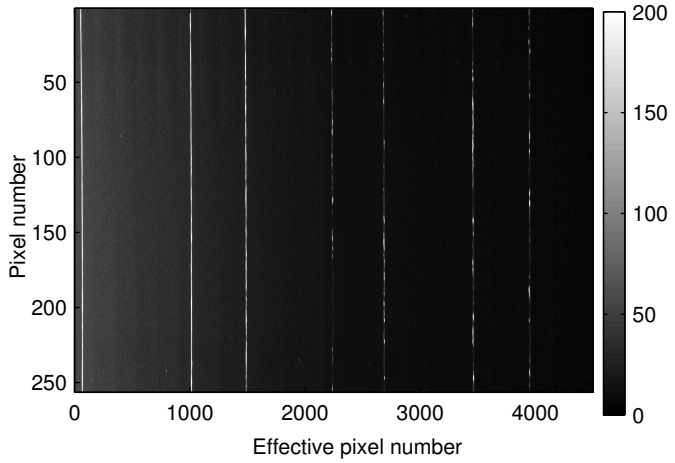

Figure 9: Image showing 7 diffraction rings, produced by combining multiple images taken by the 3D sensor. The greyscale uses a limited range, to make the weaker rings more visible. Note that the x and y axes are scaled differently.

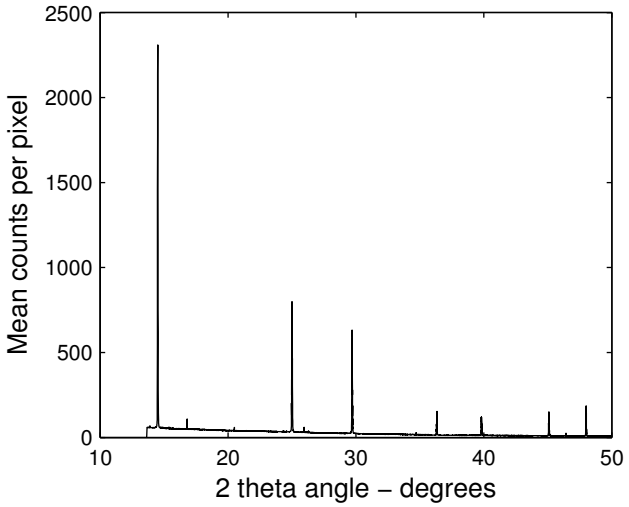

Figure 10: Powder diffraction ring intensity vs 2θ angle, obtained from images taken by 3D sensor.

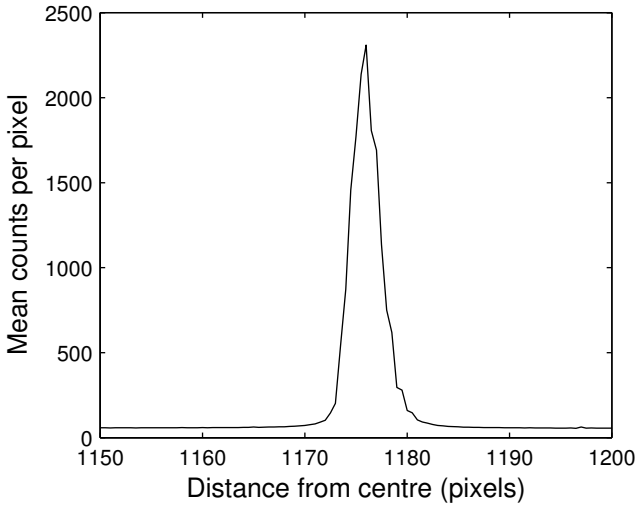

Figure 11: Profile of the first diffraction ring obtained from images taken by 3D sensor.

References

[1] E. M. Westbrook, "Performance characteristics needed for protein crystal diffraction x-ray detectors", Proc. SPIE 3774 (1999) 2–16.

[2] M. Chmeissani, B. Mikulec, "Performance limits of a single photon counting pixel system", Nucl. Instr. and Meth. A 460 (1) (2001) 81–90.

[3] S. Parker, C. Kenney, J. Segal, "3D - a proposed new architecture for solid-state radiation detectors", Nucl. Instr. and Meth. A 395 (3) (1997) 328–343.

[4] G. Pellegrini, M. Lozano, M. Ullan, R. Bates, C. Fleta, D. Pennicard, "First double-sided 3-D detectors fabricated at CNN-IMB", Nucl. Instr. and Meth A 592 (1-2) (2008) 38–43.

[5] C. Kenney, S. Parker, J. Segal, C. Storment, "Silicon detectors with 3-D electrode arrays: Fabrication and initial test results", IEEE Trans. Nucl. Sci. 46 (4) (1999) 1224–1236.

[6] C. da Via, G. Anelli, J. Hasi, P. Jarron, C. Kenney, A. Kok et al., "Advances in silicon detectors for particle tracking in extreme radiation environments", Nucl. Instr. and Meth. A 509 (1-3) (2003) 86–91.

[7] V. A. Wright, W. D. Davidson, J. J. Melone, V. O'Shea, K. M. Smith, L. Donohue et al., "Three-dimensional Medipix - a new generation of X-ray detectors", IEEE Trans. Nucl. Sci. 52 (5) (2005) 1873–1876.

[8] C. Kenney, S. Parker, E. Walckiers, "Results from 3-D silicon sensors with wall electrodes: Near-cell-edge sensitivity measurements as a preview of active-edge sensors", IEEE Trans. Nucl. Sci. 48 (6) (2001) 2405–2410.

[9] X. Llopart, M. Campbell, R. Dinapoli, D. S. Segundo, E. Pernigotti, "Medipix2: A 64-k pixel readout chip with 55mum square elements working in single photon counting mode, IEEE Trans. Nucl. Sci. 49 (5) (2002) 2279–2283.

[10] L. Tlustos, J. Kalliopuska, R. Ballabriga, M. Campbell, S. Eranen, X. Llopart, "Characterisation of a semi 3-d sensor coupled to Medipix2", Nucl. Instr. and Meth. A 580 (2) (2007) 897–901.

[11] Z. Vykydal, J. Jakubek, S. Pospisil, "USB interface for medipix2 pixel device enabling energy and position-sensitive detection of heavy charged particles", Nucl. Instr. and Meth. A 563 (1) (2006) 112–115.

[12] Diamond Light Source, B16 beamline plan, available at http://www.diamond.ac.uk/Beamlines/Beamlineplan/B16/default.htm (2008).

[13] D. Pennicard, G. Pellegrini, M. Lozano, R. Bates, C. Parkes, V. O'Shea, V. Wright, "Simulation results from double-sided 3-D detectors", IEEE Trans. Nucl. Sci. 54 (4) (2007) 1435–1443.

[14] H. Fujita, D. Y. Tsai, T. Itoh, K. Doi, J. Morishita, K. Ueda, A. Ohtsuka, "A simple method for determining the modulation transfer function in digital radiography", IEEE Trans. Med. Imaging 11 (1) (1992) 34–39.

[15] NIST, Standard Reference Materials Program.